Angewandte Chemie
Eine Zeitschrift der Gesellschaft Deutscher Chemiker

Supporting Information

Less Unfavorable Salt Bridges on the Enzyme Surface Result in More Organic Cosolvent Resistance

Haiyang Cui, Lobna Eltoukhy, Lingling Zhang, Ulrich Markel, Karl-Erich Jaeger, Mehdi D. Davari, and Ulrich Schwaneberg**

anie_202101642_sm_miscellaneous_information.pdf

Table of Contents

Analysis of the salt bridge landscape in the BSLA-SSM library toward resistance against organic solvents DOX, DMSO, and TFE

In the BSLA-SSM library, 89, 58, and 57 amino acid substitutions were identified, which exhibited increased resistance toward DOX, DMSO, and TFE, respectively, associated with the formation or disruption of a salt bridge compared to BSLA WT. As shown in **Table S1**, 58-64% (DMSO: 11/20; DOX: 9/14; TFE: 9/14) of the beneficial variants that originated from substituting one charged amino acid to another charged amino acid prefer to form a salt bridge with their neighboring residue(s). However, 53-71% (DMSO:38/70; DOX:31/44; TFE:26/43) of the uncharged to charged substitutions did not introduce new salt bridge(s). These results suggest that a balanced number of salt bridges is required within the BSLA structure to improve the OSs resistance of BSLA, which might be a prerequisite for salt bridge engineering.

In addition, analyzing the six pairs of native salt bridges in BSLA showed that only one is located in an α-helix and the remaining five in loops (**Figure S1a**, **Table S2**). In the BSLA-SSM library, the substitution landscapes at these twelve amino acid positions (i.e., 12 positions × 19 amino acid substitutions + wild-type = 229 BSLA variants; in combination with 3 OSs, this results in a total of 687 combinations of BSLA variants and OSs), show that there is no universal or predominant trend in terms of which amino acid (i.e., charged, polar, aromatic, aliphatic) improves the resistance against all three OSs (**Figure S1b**, **Table S3**). Besides, the fatality rate of substitutions at these twelve positions screened in OSs is very high (12-21%, **Table S3**). These results suggest that these salt bridge positions might not be the best candidates for enzyme engineering.

Overall structural change in each geometrical properties

The time-averaged RMSD values of all variants ranged from 1.7 Å to 2.6 Å in three OSs (DOX, DMSO, TFE) and two temperatures (25°C, 50 °C), but higher RMSD values were shown at 100°C

(3.4-4.0 Å, **Figure 4c** and **S12** in SI). The latter indicates the overall structure of BSLA remains stable in most systems except at 100°C. The corresponding results were also confirmed by examining the internal H-bond, $R_{g,}$ and SASA (**Figure S13-S15** in SI). In detail, the number of internal H-bond showed no significant change in OSs compared with water but reduced in higher temperatures (**Figure 4c** and **S13** in SI**)**. The R_g and SASA for BSLA were calculated to get insight into structural compactness changes of BSLA in six conditions. As observed in **Figure S14** in SI, the overall R_g values decrease as follows: TFE > DOX > DMSO > 100°C >50°C > Water, which agreeing well with our previous report in the case of OSs [1]. There is no significant change in SASA among different BSLA variants under each condition (**Figure S15**). But D34K/D64K in TFE shows increased total SASA and hydrophobic SASA comparing to BSLA WT.

Interestingly, we found the RMSD value increased slightly with increasing the number of substitutions in the water at 25°C, but a similar observation was not shown in OSs (e.g., DMSO and TFE) and high temperature (e.g., 100°C, **Figure 4c,** and **S12**). Aligning the stability change (e.g., RMSD, internal H-bond) of variants with their enzyme properties (OSs resistance and thermostability), the enhanced variants (e.g., D64K/D144K and D34K/D64K/D144K) had either slightly increased or slightly decreased stability comparing to BSLA WT. These results suggest balanced stability of variants in OSs and high temperature are required to improve OSs and thermal tolerance. A similar observation was also obtained by analyzing thermodynamic stability ($\Delta\Delta G_{fold}$, **Table S5**). Almost enhanced recombinants represent better instinct stabilization over WT (overall $\Delta\Delta G_{fold} < 0$), accompanying with significantly synergetic effect among each substituted amino acid (|overall $\Delta\Delta G_{fold}$ – sum $\Delta\Delta G_{fold}$ of substitutions| > 0.46 kcal/mol). Generally, salt bridges on the surface contribute less than 1 kcal/mol to the stability of the enzyme [2]. All the founding proved that there was no significant structural change among different conditions, except at 100°C. These

results can be expected because of only a few (2 to 4) surface substitutions introducing into the BSLA, which could not result in large variations in the overall dimensions comparing to BSLA WT [3].

Experimental Section

Analysis of formation and disruption of salt bridges in the BSLA-SSM library

A detailed description of the construction of the BSLA-SSM library including protein expression and the activity assay with the substrate *p*-nitrophenyl butyrate (pNPB) in 96-well MTP was reported in our previous studies [4]. The concentration of OSs 1,4-dioxane (DOX) 22 % (v/v), dimethylsulfoxide (DMSO) 60 % (v/v), 2,2,2-trifluoroethanol (TFE) 12 % (v/v) were chosen for the experiment, in which the BSLA wild-type enzyme keeps approximately 30% of its activity. The latter was proved to be a suitable condition for the screening of the "BSLA-SSM" library in previous work [4b]. The OSs mentioned above were chosen because they are frequently used in enzymatic catalysis [5]. The screening assay with OSs was performed in flat-bottomed, polystyrene 96-well MTPs (Greiner Bio-One). In each well, the crude culture supernatant (10 µL) was incubated with TEA buffer (90 µL, 50 mM, pH 7.4) or OSs solution (90 µL; 22 µL DOX + 68 µL TEA buffer, 60 µL DMSO + 30 µL TEA buffer, or 12 µL TFE + 78 µL TEA buffer) for 2 h at 25°C on the microtiter shaker (800 rpm; Edmund Bühler, Hechingen, Germany). Freshly prepared 100 µL substrate *p*NPB solution (0.5mM *p*NPB in TEA buffer with 10 % (v/v) acetonitrile) was added, and absorbance at 410 nm was monitored over 8 min on an Infinite M200 Pro microtiter plate reader (Tecan, Maennedorf, Switzerland) at room temperature. The function of acetonitrile was to dissolve *p*NPB. All the identified variants were rescreened, at least in triplicate, to determine

the improved variants. The same procedure was also performed for OS resistance profile of the purified BSLA at various concentrations. The resistance of BSLA (WT or variants) was termed as the activity ratio in the presence and absence of OS, as the following function (1):

$$\text{Residual activity } (R_{WT/V}, \%) = \frac{slope(WT/\text{variant}-Ev)\ cosolvent}{slope(WT/\text{variant}-Ev)\ buffer} \quad (1)$$

A beneficial substitution was defined as a substitution that increases BSLA resistance to the respective OS [5b]. To ensure satisfying the geometric distance and direction criteria for potential salt-bridges, oppositely charged amino acids with their C_β distances <8-10 Å were considered as "potentially salt-bridge-forming" [5b].

Generation of BSLA recombinants by mutagenesis

The recombinants were constructed by stepwise site-directed mutagenesis (SDM) [6] with the previously constructed plasmid pET22b(+)-bsla WT as the template [4a]. The primers are listed in **Table S7**. The mutants were verified by sequencing.

OS resistance profiles and kinetic characterization

The selected variants were purified according to our previous work [1]. Residual activity of purified BSLA WT and variants was measured at room temperature using *p*NPB as the substrate in the presence of various concentrations of three OSs (DOX, DMSO, TFE). Activity assays were performed at least in triplicate. The concentration of *p*NPB ranged from 0.002 to 4 mM with a fixed enzyme concentration of 1 μM. Kinetics were determined by fitting the calculated reaction rates to the Michaelis-Menten equation using software Origin pro 8.6.

Determination of thermostability profiles

Residual activity of purified BSLA variants at different temperatures was measured using the standard assay with *p*NPB as the substrate after a 60-min incubation at a varying temperature ranging from 40 to 100°C. The residual activity at room temperature (25°C) was defined as 100 %. Kinetics of thermal inactivation was monitored through incubating the purified BSLA protein

at 50 °C. Half-life (min) was defined as the time required for an enzyme variant to reach a residual activity of one half of its initial value [7].

Computational Section

In silico generation of variants and stability analysis

The BSLA crystal structure (PDB ID: 1i6w [8], Chain A, resolution 1.5 Å) was used as the template to generate the variants harboring single and multiple substitutions by the FoldX method [9] employing YASARA Plugin [10] in YASARA Structure version 17.4.17 [11]. Default parameters of FoldX (ionic strength 0.05 M; temperature 298 K; pH 7) were used. The previously reported procedure was applied to generate the 3D structure of variants [1, 12], and calculate their $\Delta\Delta G_{fold}$ ($\Delta\Delta G_{fold} = \Delta G_{fold,sub} - \Delta G_{fold,wt}$). $\Delta\Delta G_{fold}$ value is used to evaluate the thermodynamic stability of variants [12]. The larger the $\Delta\Delta G_{fold}$ negative values, the higher the stability. Five FoldX runs were performed for each variant.

Molecular dynamics simulations

Molecular dynamics (MD) simulations were performed with GROMACS v 5.1.2 software. The GROMOS96 (54a7) force field was used to simulations of BSLA variants in water and OS co-solvents as our previous work [1]. The protonation state of ionizable residues was defined based on pK_a calculation at pH 7.4 using ProteinPrepare [13]. The OS models (DOX, DMSO, TFE) were taken from our previous work with the parameter set of GROMOS96 (54a7) force field [14]. All three models are able to reproduce the properties of the water/OS solutions in perfect agreement with the experimental data [1]. Structures were solvated into a cubic box of SPCE [15] water molecules with a minimal distance of the BSLA to the borders of 1.2 nm. According to the experimental conditions (22% (v/v) DOX, 60% (v/v) DMSO, and 12% (v/v) TFE), the simulation systems were filled with ~8363 water molecules in water only system, ~280 DOX molecules and

~6950 water molecules in the DOX system, ~952 DMSO molecules, and ~4200 water molecules in the DMSO system, ~223 TFE molecules and ~7192 water molecules in TFE system, respectively.

Prior to MD simulations, energy minimization using the steepest descent method was performed to avoid the most unfavorable interactions as our previous work [1]. 100 ps NVT ensemble was completed with temperatures kept close to 298K and followed by 100 ps equilibration in the NPT ensemble with position restraints on the BSLA. The production simulation time was chosen to be 100 ns at 298 K and 1 bar in water and OSs systems (time step is 1 fs). The production temperature in 50°C and 100°C systems was chosen at 323K and 373K. To avoid artifacts, three independent MD simulation runs with different starting atomic velocities were performed. During the MD simulation, coordinates, energies, and velocities were stored every 0.5 ns for further analysis. All analyses (e.g., RMSD, internal h-bond, hydration shell, and others) were calculated by the corresponding GROMACS tools. Pymol [16] and VMD 1.9.2 [17] were applied for visualization. The salt bridge analysis tool in VMD 1.9.2 was used for analyzing the formation/ disruption of the salt bridges in MD simulations [1, 17].

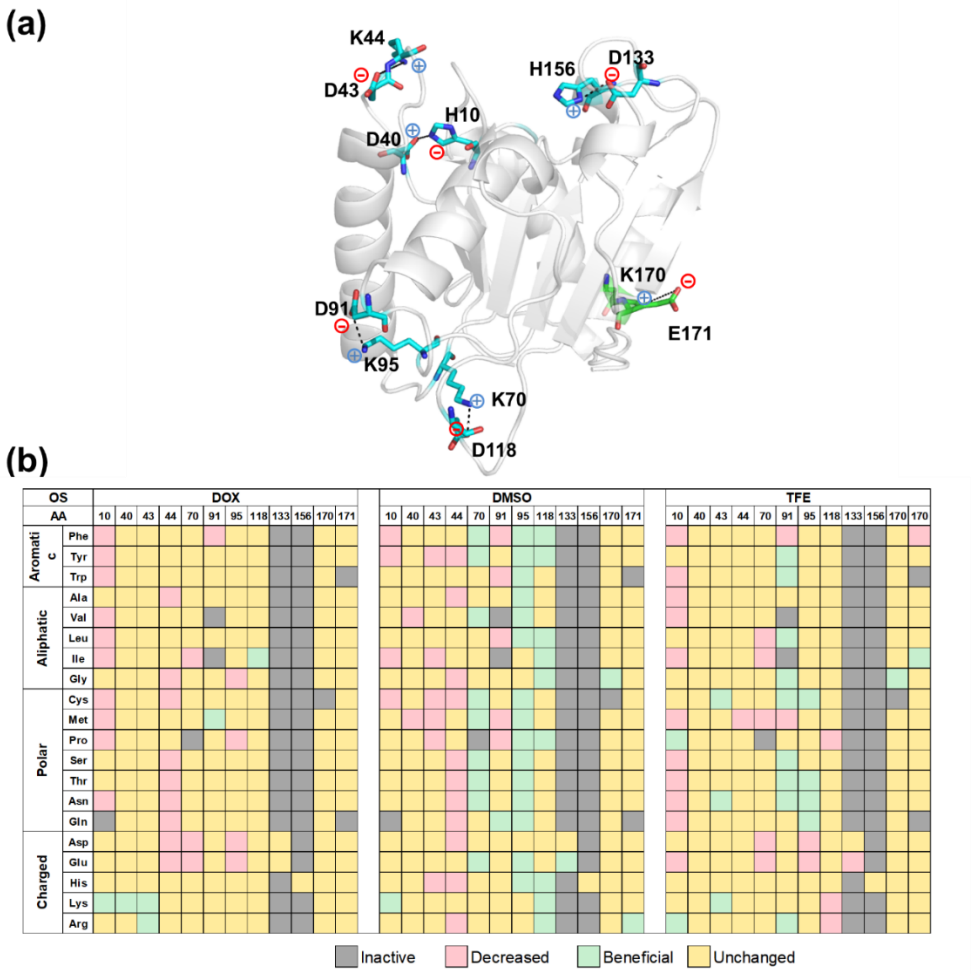

Figure S1. Analysis of substitutions landscape in instinct salt bridges. (**a**) Visualisation of instinct salt bridge in BSLA WT in water during MD simulation. Amino acids of the salt bridge on loop and helix are shown by cyan and green sticks. The salt bridge is shown with the dark dotted line. The salt bridge analysis tool in VMD 1.9.2 was applied for analyzing the formation/ disruption of the salt bridge in MD simulations [1, 17]. (**b**) OSs resistance heatmap of BSLA substitutions located on instinct salt bridges. Residual activity, activity, variants, and the empty vector are denoted as R, A, V, and EV, respectively. The variants are identified by the following four categories, dark green: beneficial substitutions with improved resistance ($R_V \geq R_{WT} + 3\sigma$); yellow: unchanged substitutions ($R_{WT} - 3\sigma < R_V < R_{WT} + 3\sigma$); pink: decreased substitutions ($R_V \leq R_{WT} - 3\sigma$); grey: non-detectable activity in buffer under assay condition ($A_V < A_{EV} + 3\sigma$). Residual activity, activity, wild-type, empty vector, variant is denoted as *R*, *A*, WT, EV, V, respectively. The OS resistance was measured in the absence or presence of 22% (v/v) DOX, 60% (v/v) DMSO, and 12% (v/v) TFE cosolvents after 2 h incubation with crude culture supernatant.

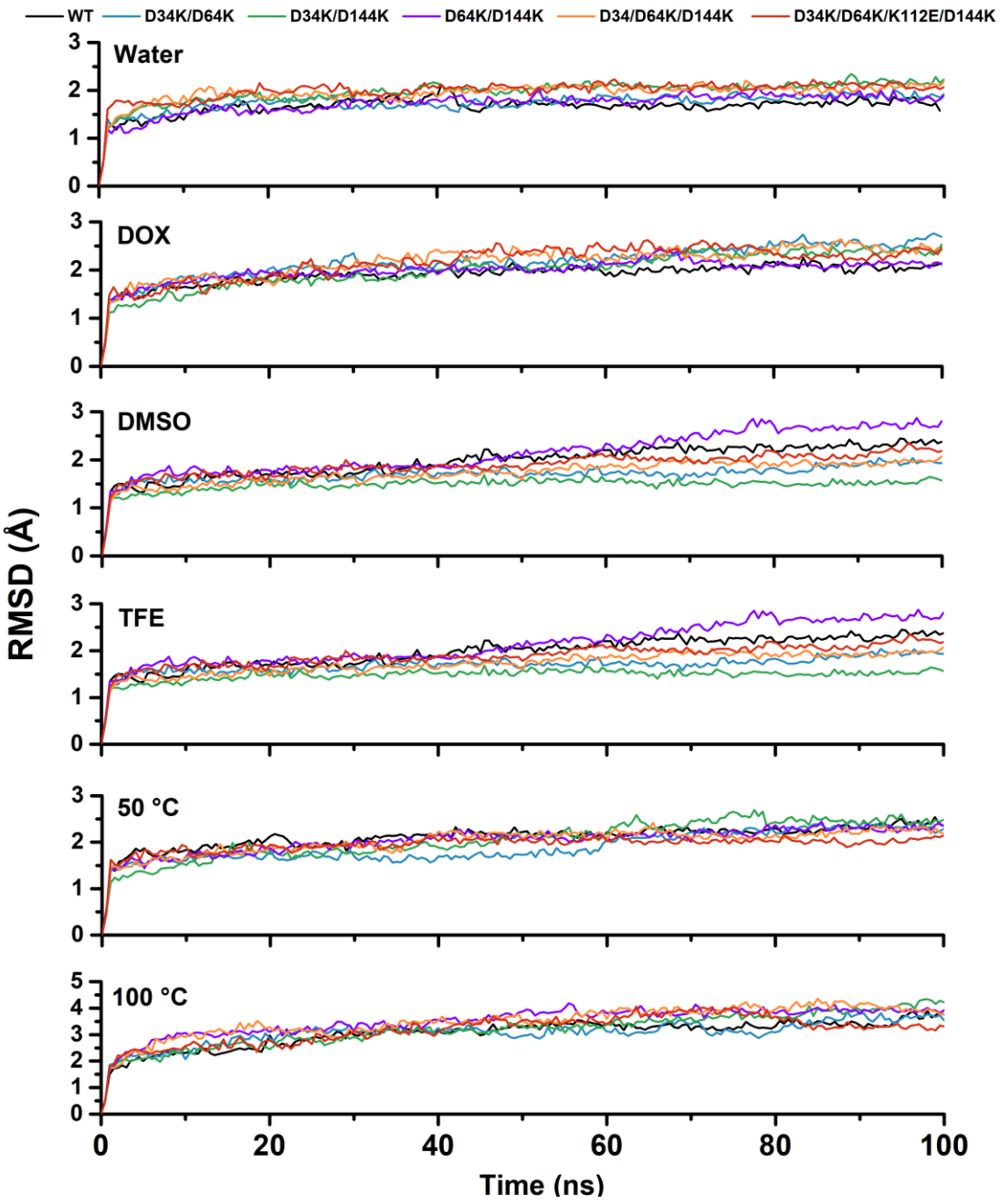

Figure S2. Root-mean-square deviation (RMSD) of the BSLA backbone with respect to the initial structure as a function of time in six conditions (water at 25°C, DOX at 25°C, DMSO at 25°C, TFE at 25°C, water at 50°C, water at 100°C). 22% (v/v) DOX, 60% (v/v) DMSO, and 12% (v/v) TFE were used. The RMSD value is average from three independent MD runs.

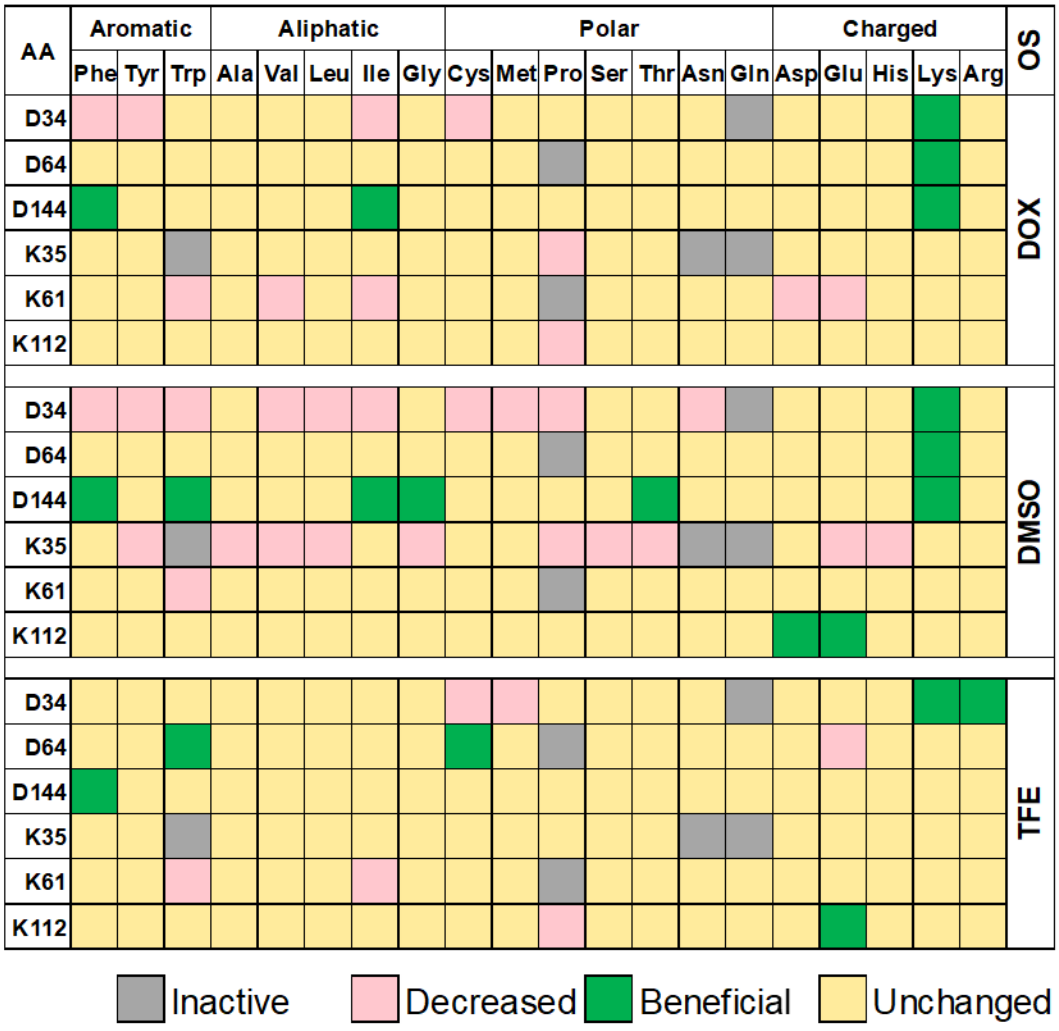

Figure S3. OSs resistance pattern of BSLA substitutions toward DOX, DMSO, and TFE at selected amino acid positions that formed three additional salt bridges. The variants are classified by the following four categories, dark green: beneficial substitutions with improved resistance ($R_V \geq R_{WT} + 3\sigma$); yellow: unchanged substitutions ($R_{WT} - 3\sigma < R_V < R_{WT} + 3\sigma$); pink: decreased substitutions ($R_V \leq R_{WT} - 3\sigma$); grey: non-detectable activity in buffer under assay condition (AV < AEV + 3σ). Residual activity, activity, wild-type, empty vector, variant is denoted as *R*, *A*, WT, EV, V, respectively. The OS resistance was measured in the absence or presence of 22% (v/v) DOX, 60% (v/v) DMSO, and 12% (v/v) TFE cosolvents after 2 h incubation with crude culture supernatant. A statistical summary of the results is given in Table 1.

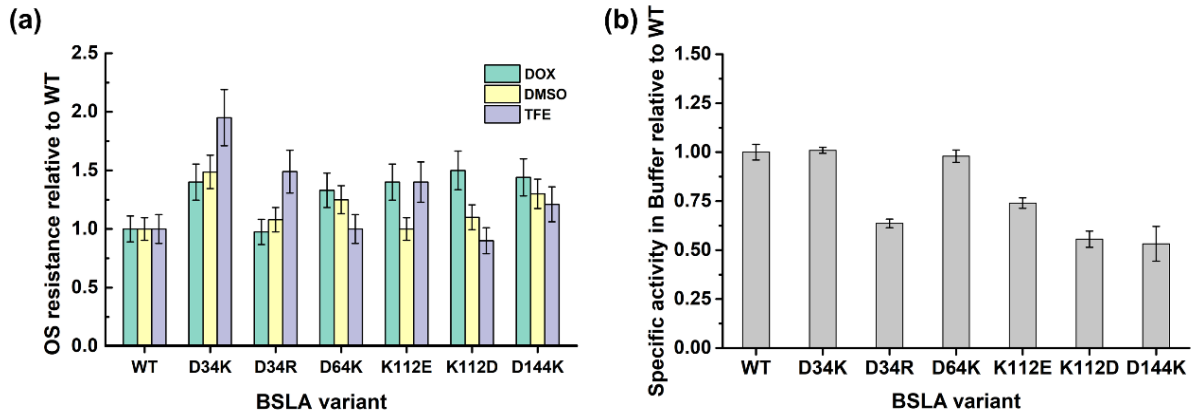

Figure S4. Performance of single BSLA substitutions. (**a**) OS resistance of single BSLA substitutions in OSs relative to BSLA WT. (**b**) The specific activity of single BSLA substitutions in buffer relative to BSLA WT. The experimental concentration of OS is 22 % (v/v), 60 % (v/v), 12 % (v/v) in DOX, DMSO, and TFE, respectively. All measurements were repeated at least three times with crude culture supernatants.

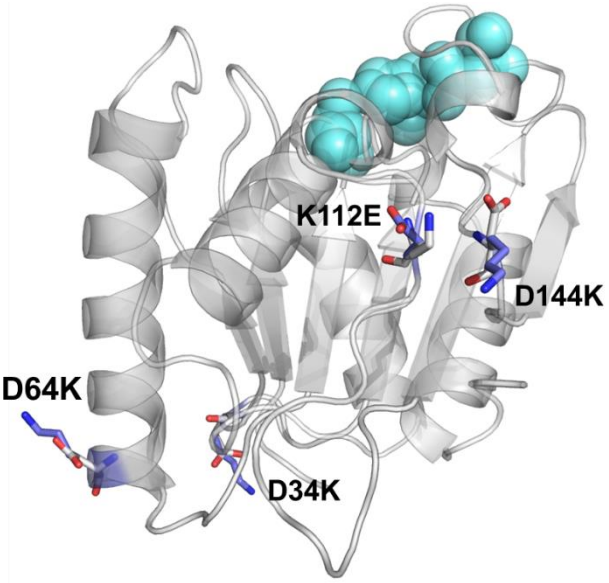

Figure S5. The positions of four selected amino acid substitutions on the BSLA structure. Cartoon representation in grey with transparency. Wild-type and substituted amino acids are shown as grey and marine sticks, respectively. The catalytic triad (S77, D133, and H156) is shown in cyan as spheres.

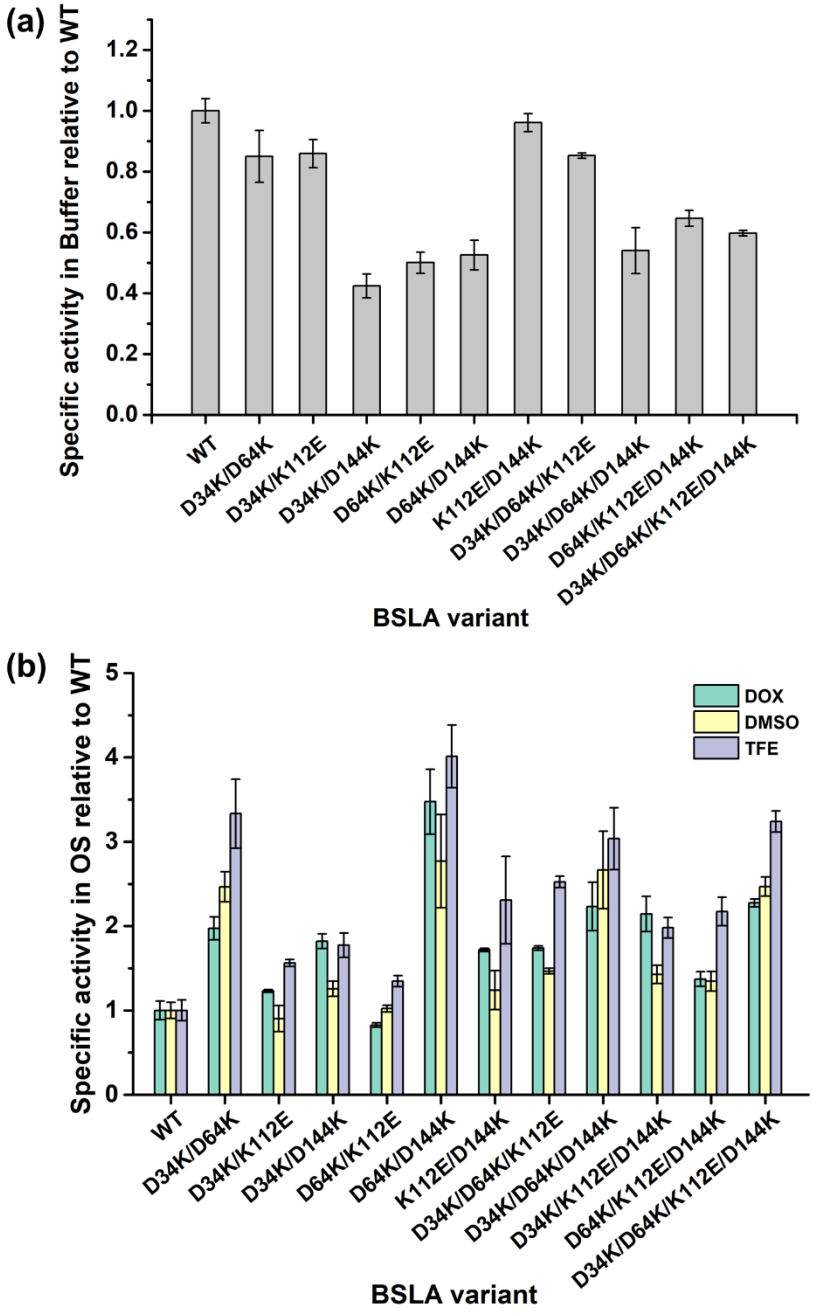

Figure S6. The specific activity of BSLA recombinants in (**a**) buffer or (**b**) OS relative to BSLA WT. Specific activity in OSs was measured under the respective OS conditions that are used in **Figure 1b**. 22% (v/v) DOX, 60% (v/v) DMSO, and 12% (v/v) TFE were used. All measurements were repeated at least three times with crude culture supernatants.

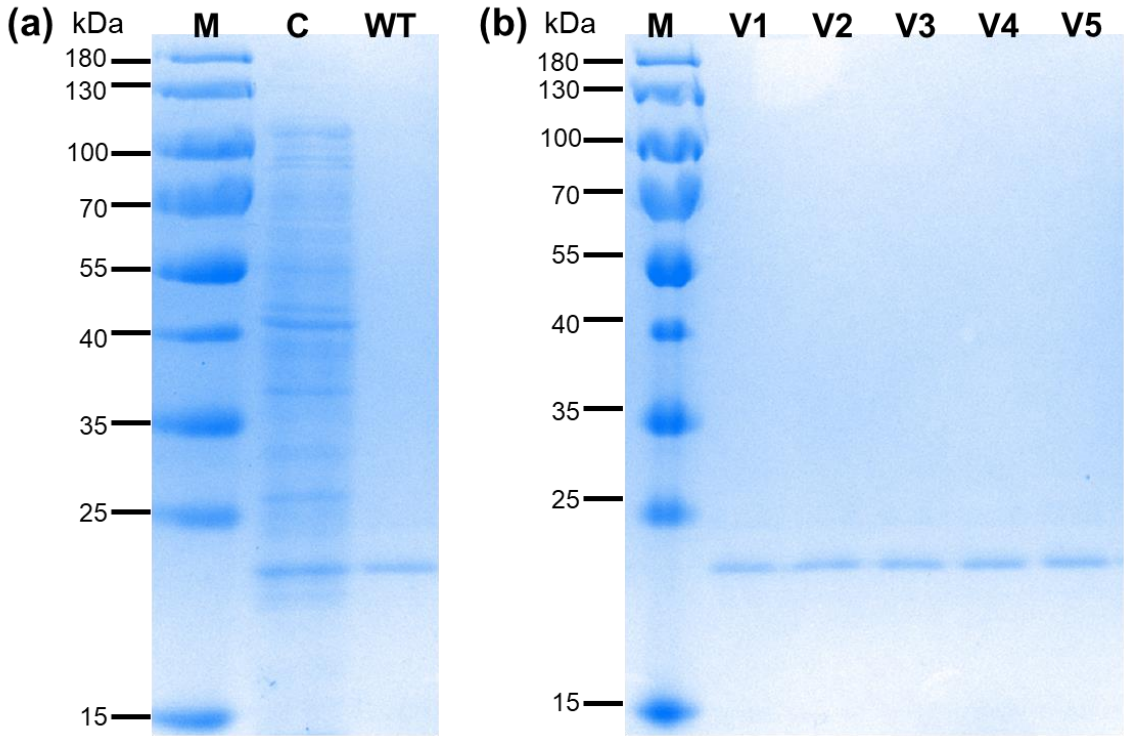

Figure S7. Identification and SDS-PAGE analysis of the purified BSLA proteins. (**a**) The BSLA WT expression and purification. M: Marker with 15-180 kDa C: the crude BSLA lysate, WT: purified BSLA wild-type. (**b**) The purified BSLA recombinants. The remaining five lanes beside Marker from left to right are D34K/D64K, D34K/D144K, D64K/D144K, D34/D64K/D144K, and D34K/D64K/K112E/D144K, respectively. The purified protein was loaded onto 5 % stacking gel and 12 % separating gel. The gel was stained with Coomassie Brilliant Blue.

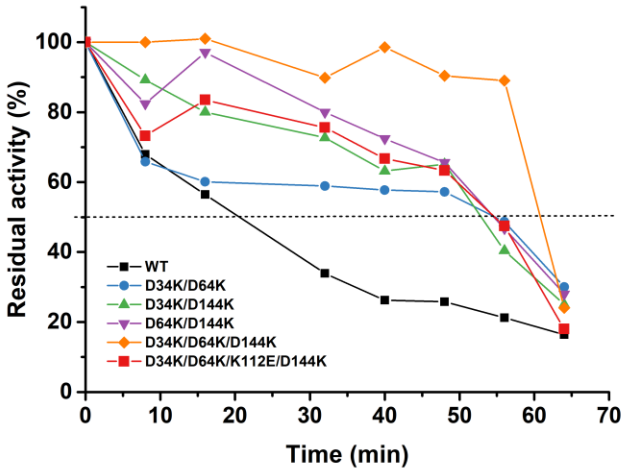

Figure S8. The residual activity of BSLA variants at 50°C as a function of time. Residual activity in buffer at the starting point was defined as 100%.

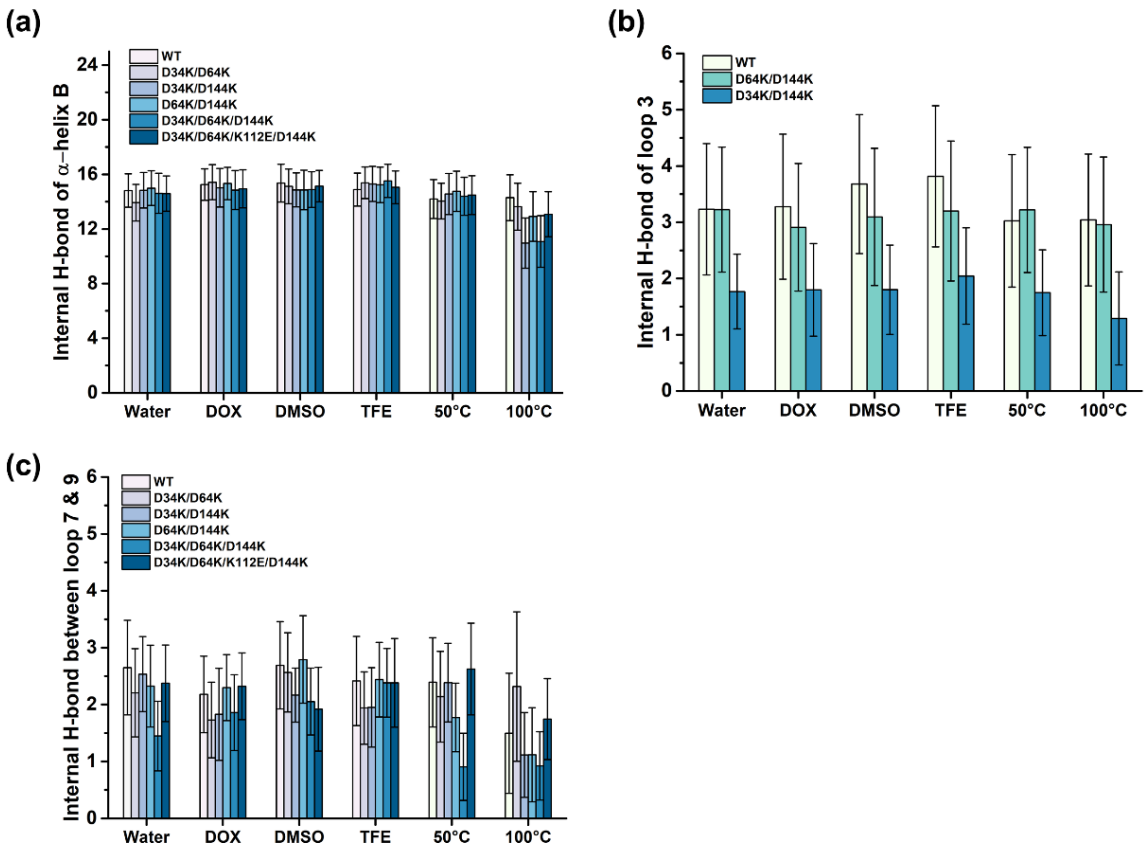

Figure S9. The number of internal hydrogen bonds with > 95% occupancy within the local region of BSLA variants determined from the last 40 ns of simulations under six conditions (water at 25°C, DOX at 25°C, DMSO at 25°C, TFE at 25°C, water at 50°C, water at 100°C). (**a**) α-helix B (residue 47-67), (**b**) Loop 3 (residue 29-35), and (**c**) Loop 7 & 9 (residue 109-124 and 142-147). Error bars describe the standard deviation from three independent MD runs. Geometric cut off for evaluation of hydrogen bond distance 3.5 Å and angle 30° were used.

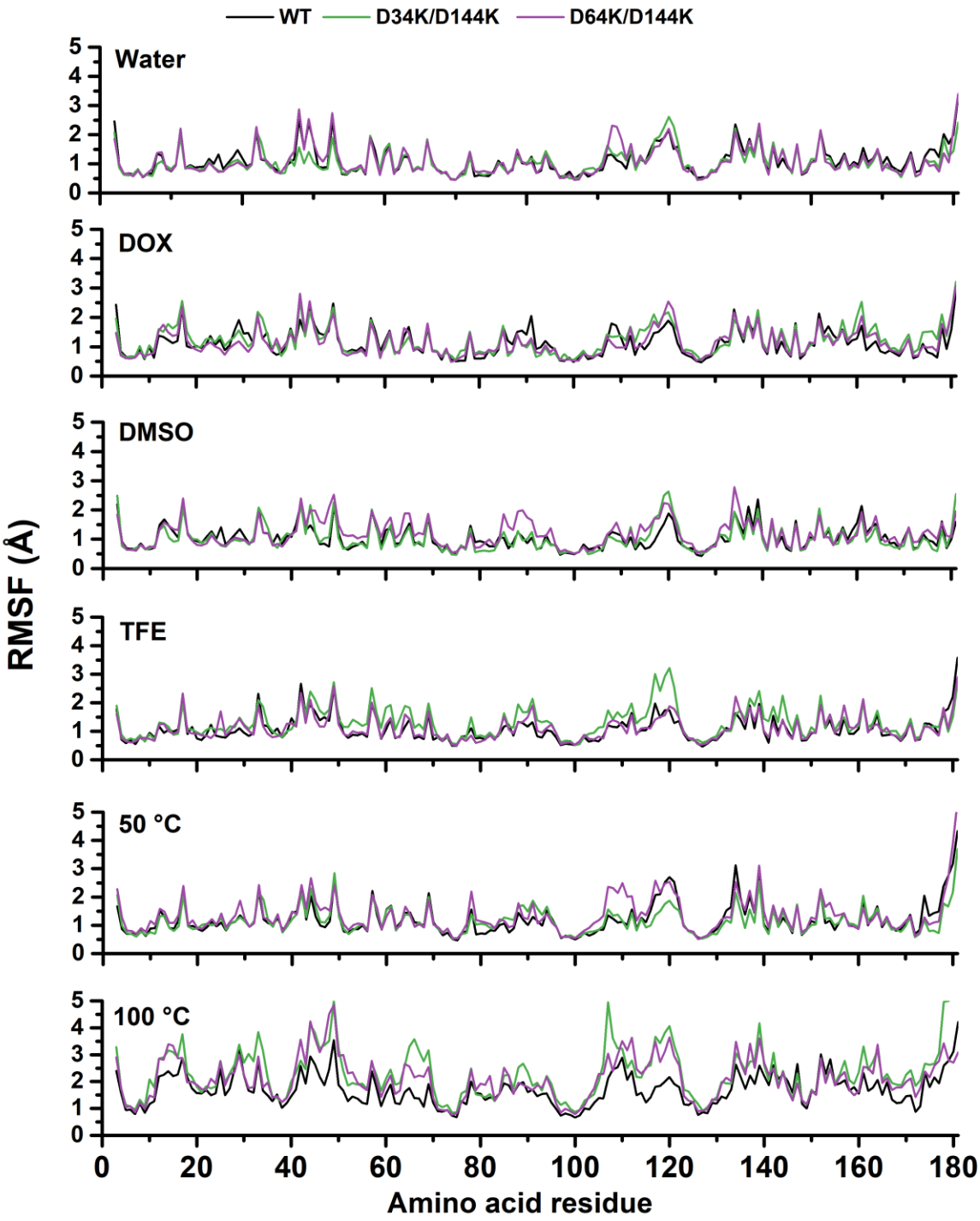

Figure S10. RMSF of BSLA residues determined from the last 40 ns of MD simulations in cosolvents and at different temperatures.

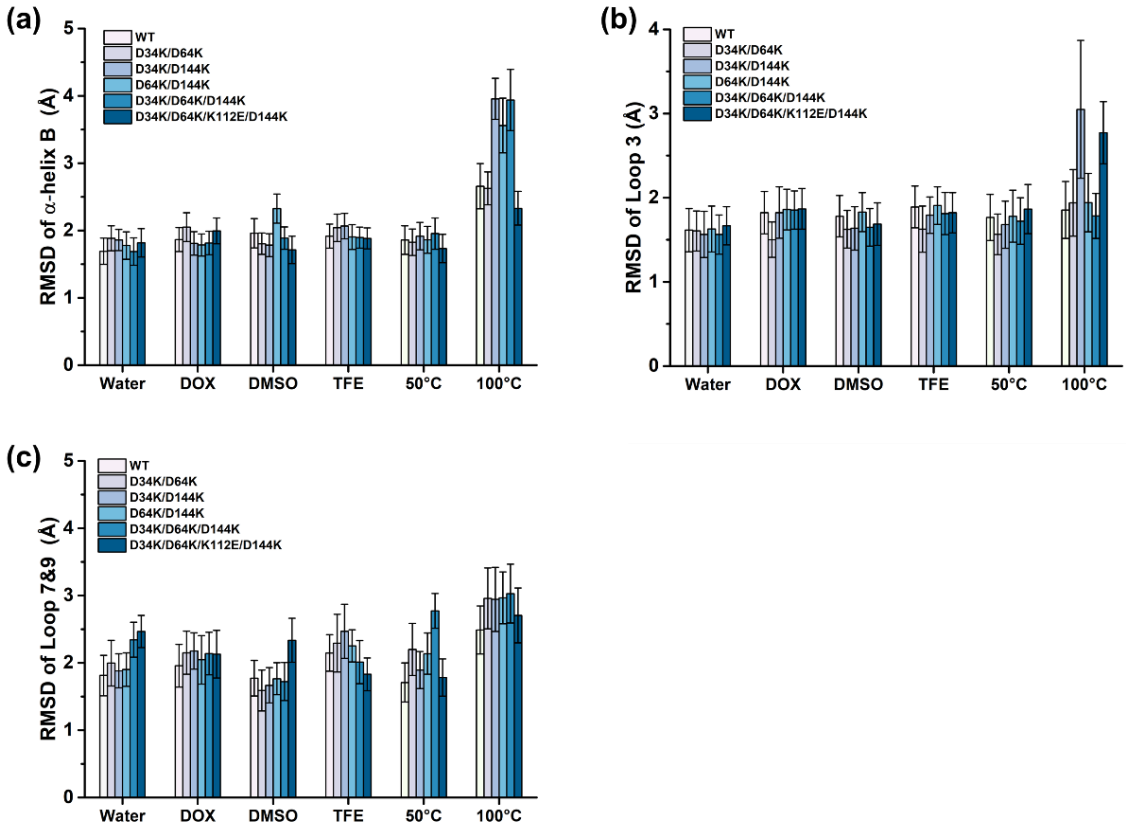

Figure S11. Time-average RMSD of the local region including extra salt bridges within BSLA variants determined from the last 40 ns of simulations under six conditions (water at 25°C, DOX at 25°C, DMSO at 25°C, TFE at 25°C, water at 50°C, water at 100°C). (**a**) α-helix B (residue 47-67), (**b**) Loop 3 (residue 29-35), and (**c**) Loop 7 & 9 (residue 109-124 and 142-147).

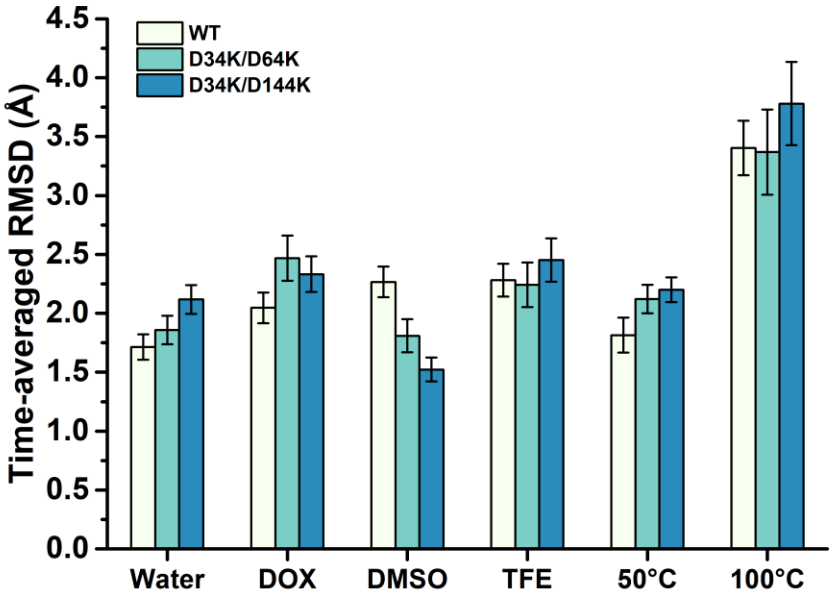

Figure S12. Time-average RMSD of the heavy atoms of BSLA variants determined from the last 40 ns of simulations under six conditions (water at 25°C, DOX at 25°C, DMSO at 25°C, TFE at 25°C, water at 50°C, water at 100°C). Error bars describe the standard deviation from three independent MD runs.

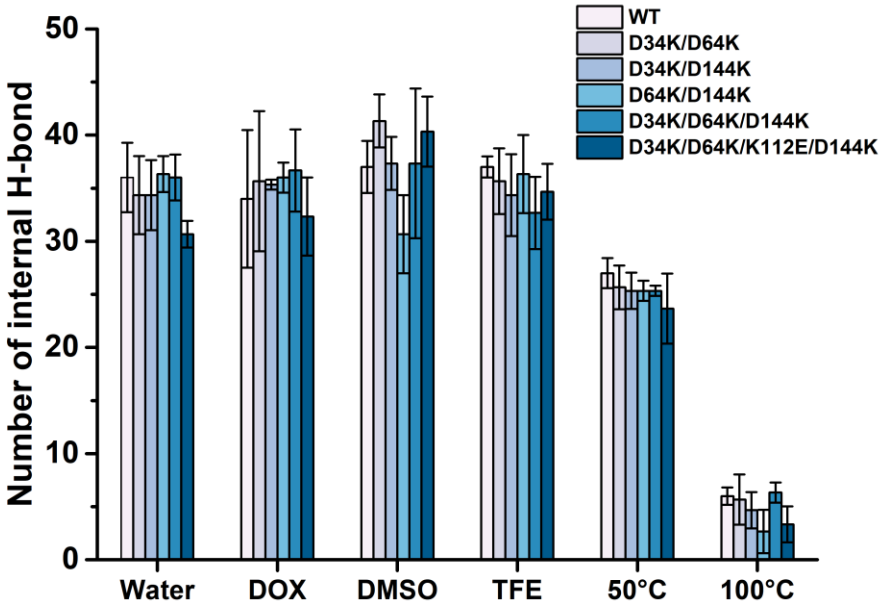

Figure S13. The number of internal hydrogen bonds with > 95% occupancy within BSLA variants determined from the last 40 ns of simulations under six conditions (water at 25°C, DOX at 25°C, DMSO at 25°C, TFE at 25°C, water at 50°C, water at 100°C). Error bars describe the standard deviation from three independent MD runs. Geometric cut off for evaluation of hydrogen bond distance 3.5 Å and angle 30° were used.

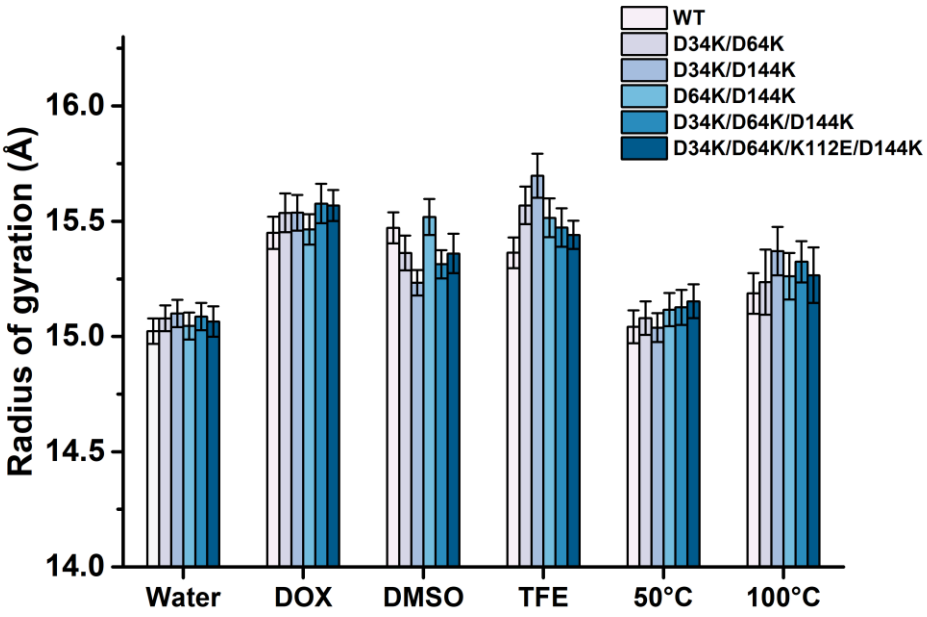

Figure S14. The time-averaged radius of gyration (R_g) of BSLA variants in six conditions. The time-averaged R_g was calculated from the last 40 ns of the MD simulations. Error bars show the standard deviation from three independent MD runs.

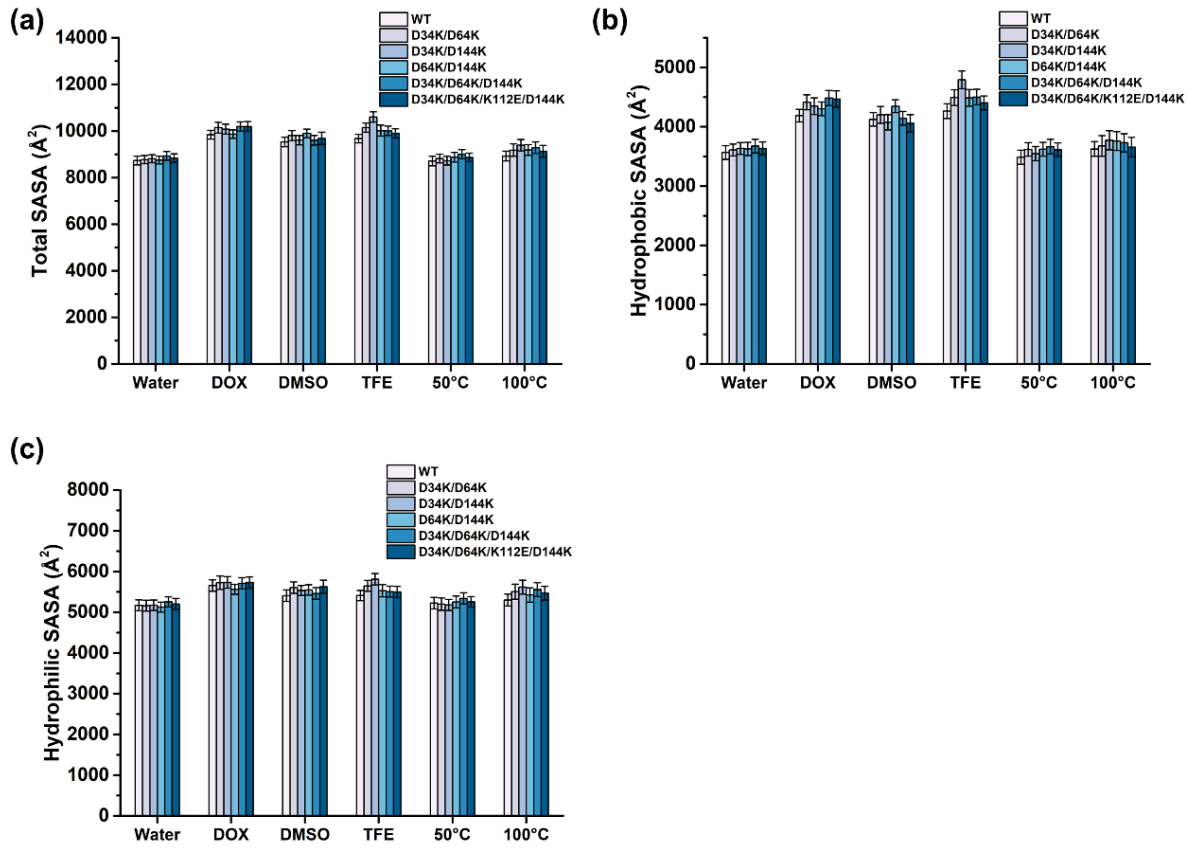

Figure S15. The time-averaged (**a**) total (**b**) hydrophobic (**c**) hydrophilic SASA of BSLA variants. The average of SASA is computed based on the last 40 ns of each simulation. Error bars show the standard deviation from three independent MD runs. Here, SASA refers to the surface area of BSLA, accessible to water molecules and OS molecules calculated using a probe of radius 1.4 Å. The cut off -0.2 to 0.2 was used for hydrophobic and hydrophilic SASA calculations [18].

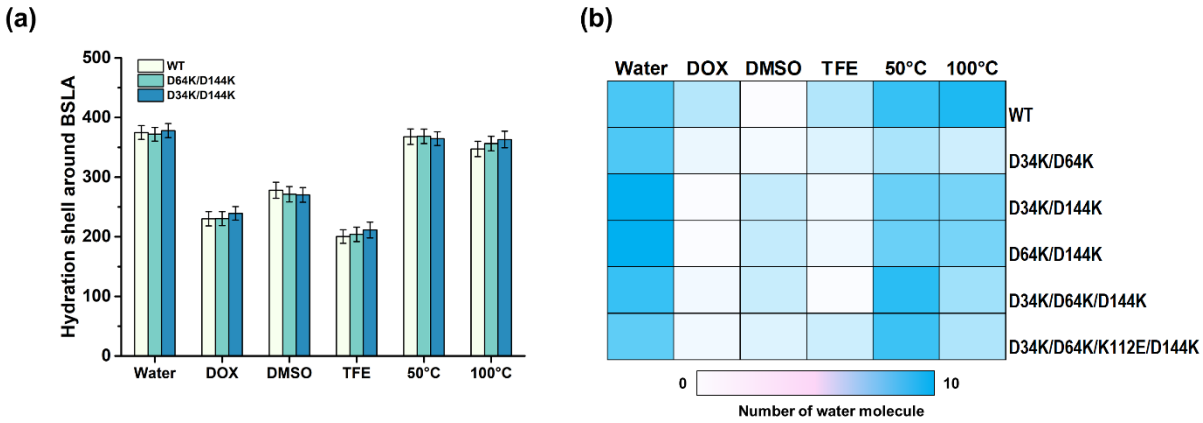

Figure S16. Hydration solvation phenomenon of BSLA variants in cosolvents and at different temperature. (**a**) Hydration shell around BSLA variants averaged over the last 40 ns of MD trajectories. The hydration shell is defined as water molecules whose oxygen atom is ≤ 3.5 Å distance cutoff of any non-hydrogen atom of protein. The number of water molecules is defined as the hydration level. (**b**) Water molecules in substrate binding cleft. The BSLA substrate binding cleft is defined as the region which expands 5.9 Å away from the bottomed Ser77 residue.

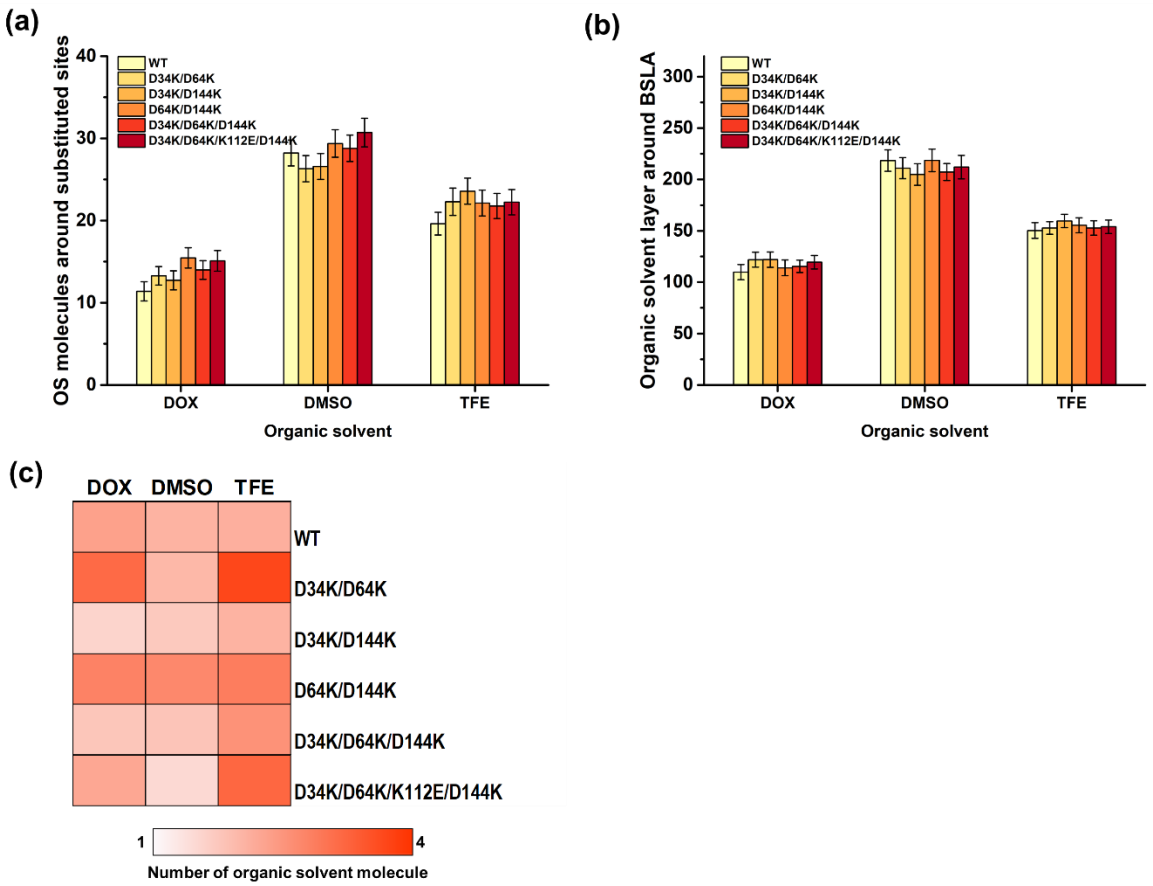

Figure S17. OS solvation phenomenon of BSLA variants in cosolvents and at different temperature. (**a**) OS molecules around the substituted sites averaged over the last 40 ns of MD trajectories. The substituted sites include positions 34, 64, 112, and 144. (**b**) OS layer averaged over the last 40 ns of trajectories. A similar definition was also applied to the OS layer. A 6.8 Å cutoff was employed for DOX, DMSO, and TFE. Error bars show the standard deviation from three independent MD runs for each system. (**c**) Number of OS molecules in BSLA substrate binding cleft averaged over the last 40 ns of trajectories. The BSLA substrate binding cleft is defined as the region which expands 5.9 Å away from the bottomed Ser77 residue.

Table S1. Analysis of the beneficial substitutions that improve the cosolvent resistance in the whole BSLA-SSM library.[a]

The fraction of beneficial substitutions % (variants)		SB[b] formed	SB[b] disruption
Charged to charged	DMSO	58% (11/20)	42% (8/20)
	DOX	64% (9/14)	36% (5/14)
	TFE	64% (9/14)	36% (5/14)
Uncharged to charged	DMSO	46% (32/70)	53% (38/70)
	DOX	30% (13/44)	71% (31/44)
	TFE	40% (17/43)	61% (26/43)

[a] 22% (v/v) DOX, 60% (v/v) DMSO, and 12% (v/v) TFE were used.

[b] SB: Salt Bridge.

Table S2. Salt bridge analysis of BSLA WT in water and OSs systems. [a]

	Water	DOX	DMSO	TFE
Salt bridge	D40-H10	D40-H10	D40-H10	-
	D43-K44	D40-K44	-	D40-K44
	D91-K95	D91-K95	D91-K95	D91-K95
	D118-K70	D118-K70	D118-K70	K118-K70
	E171-K170	E171-K170	E171-K170	E171-K170
	D133-H156	D133-H156	D133-H156	D133-H156
		D34-K35	D34-K35	D34-K35
		D64-K61	D64-K61	D64-K61
		D144-K112	D144-K112	D144-K112

[a] The data were reanalyzed from our previous study [5b].

Table S3. Classification of BSLA substitutions on the forming instinct salt bridge in OSs.[a]

OS resistance		Classification of amino acid substitution % (variant)			
		Aromatic	Aliphatic	Polar	Charged
DOX	Beneficial	0	2 % (1)	1 % (1)	8 % (5)
	Unchanged	70 % (25)	66 % (40)	66 % (55)	72 % (43)
	Decreased	11 % (4)	12 % (7)	12 % (10)	10 % (6)
	Inactive	19 % (7)	20 % (12)	21 % (18)	12 % (7)
DMSO	Beneficial	19 % (7)	13 % (8)	17 % (14)	15 % (9)
	Unchanged	44 % (16)	57 % (34)	48 % (40)	66 % (40)
	Decreased	17 % (6)	10 % (6)	14 % (12)	7 % (4)
	Inactive	19 % (7)	20 % (12)	21 % (18)	12 (7)
TFE	Beneficial	6 % (2)	7 % (4)	13 % (11)	5 % (3)
	Unchanged	64 % (23)	65 % (39)	56 % (47)	70 % (42)
	Decreased	11 % (4)	8 % (5)	11 % (9)	13 % (8)
	Inactive	19 % (7)	20 % (12)	20 % (17)	12 % (7)

[a] The amino acid positions 10, 40, 43, 44, 70, 91, 95, 118, 133,156, 170, and 171 were selected for statistical analysis. OSs include 22 % (v/v) DOX, 60 % (v/v) DMSO, and 12 % (v/v) TFE.

Table S4. Kinetic characterization of BSLA variants in (co)solvents.

BSLA variant	Buffer[a]			DOX[b]			DMSO[b]			TFE[b]		
	K_M (mM)	k_{cat} (min^{-1})	k_{cat}/K_M (mM^{-1} min^{-1})	K_M (mM)	k_{cat} (min^{-1})	k_{cat}/K_M (mM^{-1} min^{-1})	K_M (mM)	k_{cat} (min^{-1})	k_{cat}/K_M (mM^{-1} min^{-1})	K_M (mM)	k_{cat} (min^{-1})	k_{cat}/K_M (mM^{-1} min^{-1})
WT	0.51	162	318	0.57	84	147	0.65	74	114	0.78	124	159
D34K/D64K	2.30	339	147	4.84	234	48	4.68	136	29	4.06	364	90
D34K/D144K	0.53	73	138	0.43	28	65	0.66	23	35	0.78	105	135
D64K/D144K	0.18	47	261	0.15	19	127	0.33	17	52	0.66	87	132
D34K/D64K/D144K	1.42	109	77	0.84	39	46	0.83	21	25	0.96	120	125
D34K/D64K/K112E/D144K	0.16	39	244	0.11	17	155	0.43	15	35	0.50	89	178

[a] 50 mM triethanolamine, pH 7.4

[b] 22 % (v/v) DOX, 60 % (v/v) DMSO, and 12 % (v/v) TFE

Table S5. Stability analysis of the BSLA variants.[a]

BSLA variant	Sum $\Delta\Delta G_{fold}$ of substitutions (kcal/mol)	Overall $\Delta\Delta G_{fold}$ of recombinant (kcal/mol)
D34K/D64K	−1.22	−1.04
D34K/D144K	+0.78	+0.02
D64K/D144K	+0.34	−0.84
D34K/D64K/D144K	−1.22	−0.83
D34K/D64K/K112E/D144K	+0.58	−0.52

[a] The command (Mutate residue) was applied to calculate the $\Delta\Delta G_{fold}$ of every single substitution. Sum $\Delta\Delta G_{fold} = \Delta\Delta G_{fold,sub1} + \Delta\Delta G_{fold,sub2} + \Delta\Delta G_{fold,sub3} + \Delta\Delta G_{fold,subX}$. The command (Mutate multiple residues)was applied to calculate the overall $\Delta\Delta G_{fold}$ of recombinants. Due to the accuracy of the FoldX method in the prediction of relative folding free energies is reported to be 0.46 kcal/mol, and we defined that the synergistic effect occurs when (Sum of $\Delta\Delta G_{fold}$ – Overall $\Delta\Delta G_{fold}$) > 0.46 kcal/mol. The $\Delta\Delta G_{fold}$ calculations were performed five times and averaged for each variant overall $\Delta\Delta G_{fold}$ of recombinants.

Table S6. Averaged-RMSF at the local region of the BSLA variants. [a]

		Averaged-RMSF (Å)					
Condition	Local region	WT	V1	V2	V3	V4	V5
Water	Loop3	1.28	1.31	1.29	1.26	1.21	1.34
	Loop 7 & 9	1.25	1.30	1.29	1.38	1.35	1.32
	a-helix B	1.09	1.21	1.17	1.06	1.15	1.17
DOX	Loop3	1.54	1.36	1.46	1.51	1.22	1.48
	Loop 7 & 9	1.20	1.33	1.36	1.44	1.32	1.31
	a-helix B	1.22	1.22	1.23	1.15	1.14	1.24
DMSO	Loop3	1.24	1.26	1.17	1.28	1.17	1.25
	Loop 7 & 9	1.05	1.23	1.24	1.23	1.27	1.48
	a-helix B	1.08	1.20	1.15	1.08	1.45	1.12
TFE	Loop3	1.22	1.40	1.34	1.47	1.22	1.38
	Loop 7 & 9	1.24	1.61	1.26	1.73	1.19	1.07
	a-helix B	1.16	1.30	1.21	1.55	1.21	1.09
50°C	Loop3	1.30	1.33	1.56	1.39	1.44	1.89
	Loop 7 & 9	1.39	1.55	1.51	1.26	1.62	1.24
	a-helix B	1.23	1.29	1.38	1.25	1.30	1.29
100°C	Loop3	2.09	2.23	1.85	3.00	2.22	2.20
	Loop 7 & 9	2.02	2.55	2.11	2.49	2.35	1.97
	a-helix B	1.67	2.14	2.24	2.59	2.48	1.72

[a] D34K/D64K, D34K/D144K, D64K/D144K, D34/D64K/D144K, and D34K/D64K/K112E/D144K was denoted as V1, V2, V3, V4, and V5, respectively. Loop 3 includes residue 29-35, α-helix B includes residue 47-67, and Loop 7 & 9 includes residue 109-124 and 142-147.

Table S7. Primers used for iterative site directed mutagenesis studies.

Name	5 --> 3 sequence[a]
D34K Forward Primer	GGCTGGTCGCGGAAGAAGCTGTATGCA
D34K Reverse Primer	TGCATACAGCTTGTCCCGCGACCAGCC
D34R Forward Primer	GGCTGGTCGCGGAGGAAGCTGTATGCA
D34R Reverse Primer	TGCATACAGCTTCCTCCGCGACCAGCC
D64K Forward Primer	CAAAAGGTTTTAAAGGAAACGGGTGCGA
D64K Reverse Primer	TCGCACCCGTTTCCTTTAAAACCTTTTG
K112E Forward Primer	TTGACGACAGGCGAGGCGCTT
K112E Reverse Primer	AAGCGCCTCGCCTGTCGTCAA
K112D Forward Primer	TTGACGACAGGCGATGCGCTT
K112D Reverse Primer	AAGCGCATCGCCTGTCGTCAA
D144K Forward Primer	TTATCAAGATTAAAGGGTGCTAGAA
D144K Reverse Primer	TTCTAGCACCCTTTAATCTTGATAA

[a] Mutated codon is underlined.

References

[1] H. Cui, T. H. Stadtmüller, Q. Jiang, K. E. Jaeger, U. Schwaneberg, M. D. Davari, *ChemCatChem* **2020**, *12*, 4073.

[2] a) A. Yenenler, A. Venturini, H. C. Burduroglu, O. U. Sezerman, *J. Mol. Biol.* **2018**, *24*, 229; b) D. N. Marti, H. R. Bosshard, *J. Mol. Biol.* **2003**, *330*, 621-637.

[3] L. Zhang, H. Cui, G. V. Dhoke, Z. Zou, D. F. Sauer, M. D. Davari, U. Schwaneberg, *Chem. Eur. J* **2020**, *26*, 4974-4979.

[4] a) V. J. Frauenkron-Machedjou, A. Fulton, J. Zhao, L. Weber, K. E. Jaeger, U. Schwaneberg, L. Zhu, *Bioresour. Bioprocess.* **2018**, *5*, 2; b) V. J. Frauenkron-Machedjou, A. Fulton, L. Zhu, C. Anker, M. Bocola, K. E. Jaeger, U. Schwaneberg, *ChemBioChem* **2015**, *16*, 937-945.

[5] a) A. M. Duarte, C. P. van Mierlo, M. A. Hemminga, *J. Phys. Chem. B* **2008**, *112*, 8664-8671; b) U. Markel, L. Zhu, V. J. Frauenkron-Machedjou, J. Zhao, M. Bocola, M. D. Davari, K. E. Jaeger, U. Schwaneberg, *Catalysts* **2017**, *7*, 142.

[6] L. J. Strategene, California, *Instruction Manual* **2003**.

[7] a) V. Stepankova, S. Bidmanova, T. Koudelakova, Z. Prokop, R. Chaloupkova, J. Damborsky, *ACS Catal.* **2013**, *3*, 2823-2836; b) Y. Zhou, B. Pérez, W. Hao, J. Lv, R. Gao, Z. Guo, *Biochem. Eng. J.* **2019**, *148*, 195-204.

[8] G. van Pouderoyen, T. Eggert, K. E. Jaeger, B. W. Dijkstra, *J. Mol. Biol.* **2001**, *309*, 215-226.

[9] J. Schymkowitz, J. Borg, F. Stricher, R. Nys, F. Rousseau, L. Serrano, *Nucleic Acids Res.* **2005**, *33*, W382-W388.

[10] J. Van Durme, J. Delgado, F. Stricher, L. Serrano, J. Schymkowitz, F. Rousseau, *Bioinformatics* **2011**, *27*, 1711-1712.

[11] E. Krieger, G. Koraimann, G. Vriend, *Proteins: Struct., Funct., Bioinf.* **2002**, *47*, 393-402.

[12] H. Cui, H. Cao, H. Cai, K. E. Jaeger, M. D. Davari, U. Schwaneberg, *Chem. Eur. J* **2020**, *26*, 643-649.

[13] G. Martínez-Rosell, T. Giorgino, G. De Fabritiis, *J. Chem. Inf. Model.* **2017**, *57*, 1511-1516.

[14] A. K. Malde, L. Zuo, M. Breeze, M. Stroet, D. Poger, P. C. Nair, C. Oostenbrink, A. E. Mark, *J. Chem. Theory Comput.* **2011**, *7*, 4026-4037.

[15] P. Mark, L. Nilsson, *J. Phys. Chem. A* **2001**, *105*, 9954-9960.

[16] W. L. DeLano, *http://www.pymol.org* **2002**.

[17] W. Humphrey, A. Dalke, K. Schulten, *J. Mol. Graph.* **1996**, *14*, 33-38.

[18] F. Eisenhaber, P. Lijnzaad, P. Argos, C. Sander, M. Scharf, *J. Comput. Chem.* **1995**, *16*, 273-284.